Biointerface Research in Applied Chemistry
Open-Access Journal (ISSN: 2069-5837)

Article
Volume 13, Issue 6, 2023, 582
https://doi.org/10.33263/BRIAC136.582

Assessment of the Functionalization of Chitosan/ Iron Oxide Nanoparticles

Asmaa M. Ismail [1], Taha M.Tiama [2], Ahmed Farghaly [3], Hanan Elhaes [4], Medhat A. Ibrahim [1,*]

[1] Molecular Spectroscopy and Modeling Unit, Spectroscopy Department, National Research Centre, 33 El-Bohouth St., 12622, Dokki, Giza, Egypt
[2] Basic Science Department, October High Institute for Engineering & Technology, 6th October City, Cairo, Egypt
[3] X-Ray Crystallography Lab., Solid State Physics Department, National Research Centre, 33 El-Bohouth St., 12622, Dokki, Giza, Egypt
[4] Physics Department, Faculty of Women for Arts, Science and Education, Ain Shams University, 11757 Cairo, Egypt
* Correspondence: medahmed6@yahoo.com (M.A.I.);

Scopus Author ID 8641587100
Received: 11.10.2022; Accepted: 30.11.2022; Published: 2.04.2023

Abstract: A composite of chitosan and chitosan with Fe_3O_4 (5, 10, 15 and 20 wt%) is casted forming film. At room temperature, prepared samples were analyzed with ATR-FTIR spectroscopy, X-ray diffraction (XRD), and a vibrating sample magnetometer (VSM). Then, antimicrobial activity against different microorganisms was evaluated. ATR-FTIR results showed that the bands for chitosan/Fe_3O_4 at 3250 cm^{-1} of the O-H band become broader compared to pure chitosan. Fe_3O_4 shows bands at 3195 cm^{-1} and 1628 cm^{-1} related to O-H stretching and bending. Magnetite Fe_3O_4 has two strong infrared absorption bands at 547 cm^{-1} and 435 cm^{-1}. X-ray diffraction results confirmed the reaction and showed that a 10% weight percentage is the most reactive ratio consistent with FTIR results. The crystallinity index and crystallite size increase with increasing the concentration of magnetite, indicating that the samples prefer the amorphous form at the low concentrations of Fe_3O_4, and they rearrange towards the crystalline state due to the presence of magnetite. Magnetic measurements showed that both saturation magnetizations (Ms) and remanent magnetizations (Mr) increase while the coercive field (Hc) first decreases and then increases as the Fe_3O_4 concentration increases in the prepared nanocomposites. From antimicrobial activity against different microorganisms results, chitosan/Fe_3O_4 with different weight percentages of Fe_3O_4 showed strong antibacterial activity against bacterial species.

Keywords: chitosan/Fe_3O_4; ATR-FTIR; XRD; VSM and antimicrobial activity.

1. Introduction

Beyond any doubt, the development of nanotechnology has provided many resources for various applications in the medical field, for example, in the field of diagnosis, biological detection, treatment, and drug delivery [1-5]. In this research context, magnetic nanoparticles have many important properties that make them attractive for a wide variety of biomedical applications, cell detection and separation [6,7], and the treatment of hyperthermia [8]. We find that magnetic iron oxide nanoparticles (IONPs) possess stable physical and chemical properties, making them biocompatible, environmentally safe [9], and have clinical applications. When IONPs (Fe_3O_4 (magnetite) or Fe_2O_3 (magnetite)) reach smaller sizes (about 10-20 nm iron oxide), higher magnetic properties become apparent so that the particles reach better performance for most of the aforementioned applications [10, 11].

Chitosan and its products can interact safely with live cells without negative effects on the body. [12]. Mixed with other polymers and metal nanocomposites, chitosan is used in many biomedical applications, including wound dressings, as an antimicrobial, antibacterial, and antifungal [13]. In addition to the biological applications, the unique hydrogen bonding in the chitosan dedicates it to versatility, selectivity, and large adsorption capability, making it a good candidate for water treatment [14, 15]. With the help of iron oxide, chitosan could be prepared as a microsphere to remediate Cr [16]. Again, the amazing applications of chitosan-coated with iron oxide are effectively applied against the human colorectal carcinoma (HCT-116) cell line [17]. It is stated that chitosan-coated with magnetic nanoparticles is likely to be adsorbed by normal tissues according to their circulation route based on their mucoadhesive and bioadhesive features [18].

Iron oxide nanoparticles are modified by adding polymers for biocompatibility and biostability [19]. Therefore, the polymer matrix provided in this modification has significant advantages in biomedical applications [20]. This provides a surface that facilitates access to biomolecular coupling through bio-coupling chemistry developed for biomedical applications [21].

Researchers have proven that iron oxide nanoparticles have antimicrobial properties depending on three factors, size, stability, and concentration in the growth medium [22]. However, they were found to suffer from clumping during preparation, which reduces their effectiveness in terms of inhibiting bacterial growth. Therefore, they must be coated with biocompatible and non-toxic polymers to avoid this caking [23, 24].

Chitosan has become a popular material for medical applications in recent years, especially when it is used with magnetic nanoparticles [25]. Chitosan is used along with iron oxide nanoparticles as a stabilizer due to its excellent film-forming ability, mechanical strength, biocompatibility, non-toxicity, high permeability to water, sensitivity to chemical modifications, and antibacterial properties [26]. Chitosan-coated iron oxide was irradiated by ultrasonic then the crystallinity, stability, biocompatibility, and magnetic properties were studied. Results indicated that above 70% of cells were viable with increasing concentration [27]. Further enhancement for the role of chitosan-coated with iron oxide is achieved by graphene quantum dots to act as a magnetic imaging agent [28]. Rather than biomedical applications, chitosan-coated with iron oxide show an application in the mitigation of drought stress and growth stimulant in peppermint [29]. Ag NPs/chitosan-agarose composite, which functionalized core-shell type Fe_3O_4 nanoparticles, was reported as novel anticancer studies against liver and lung cancer cells [30]. Chitosan/iron oxide shows an emerging application in the field of ophthalmology research. It shows the efficient application as a green catalyst [31]. It also could act as an active photocatalytic removing agent [32]. Show the ability to remove dye as well as mercury from the aquatic environment [33].

Based upon the above considerations, the current study is conducted to prepare and functionalize Chitosan/Fe_3O_4 nanocomposites. So, the prepared samples' structural, magnetic properties, and antimicrobial activity were studied against various microorganisms.

2. Materials and Methods

2.1. Magnetite nanoparticle preparation.

$FeSO_4.7H_2O$ extra pure from Sham Lab, $FeCl_3.5H_2O$ anhydrous LR, and NH_4OH (25 wt% NH_3 in water) from Laboratory Rasayan were used to prepare magnetite in the form

of powder. A solution of $FeSO_4.7H_2O$ (2.8gm/150ml distilled water) (1M) was prepared with stirring at 70 °C for 30 min. A solution of $FeCl_3.5H_2O$ (3.25gm/100ml distilled water) (2M) was prepared with stirring at 70 °C for 30 min. A mixture of 0.1 M of $FeCl_3$ and $FeSO_4$ solution was made with continuous stirring at 70 °C and a quick addition of a solution of NH_4OH (10 V%) of pH =10. Immediately, a dark magnetite precipitate was formed and left to dry for 24 hrs at 40 ºC.

2.2. Cs/Fe_3O_4 nanocomposite preparation.

A medium molecular weight Aldrich chitosan powder prepared the proposed homogenous films. Appropriate weight of chitosan was dissolved in 98 ml of DI water and 2 ml acetic acid under stirring at 60ºC for 4 hrs until a homogenous viscous solution was formed. Different weight percentages of Fe_3O_4 (5, 10, 15, and 20 wt%) were added to the chitosan solution, as presented in Table 1. The solution was magnetically stirred for 6 hrs and sonicated (by using 450 Sonifier) for 1 hr to prevent the agglomeration of the nanoparticles. The nanocomposite solution was cast in a plastic petri dish and left to dry for 24 hrs at 40 ºC. The films were about 20 μm in thickness.

Table 1. Composition as the weight percentage of the studied chitosan/ Fe_3O_4.

Sample	Chitosan Wt %	Fe_3O_4 Wt %
S1	100	0
S2	95	5
S3	90	10
S4	85	15
S5	80	20
S6	0	100

2.3. Antibacterial activities for chitosan/Fe_3O_4 nanocomposite preparation.

Antibacterial activities of the synthesized Cs/Fe_3O_4 nanocomposite were performed against pathogenic bacteria. The antimicrobial activity of the tested compounds was determined by means of the agar diffusion method on Muller Hinton agar. The wells (8 mm diameter) were cut using a sterile cork borer on Muller Hinton agar (MHA, India). Twenty-four hours young cultures of antimicrobial activity against two Gram-negative (*Escherichia coli*, *Bacillus subtilis*) and two Gram-positive bacteria (*Staphylococcus aureus*, *Salmonella typhi*) were studied. The samples were swabbed with sterilized cotton swabs on the surface of prepared Muller Hinton agar. One hundred microliters of compounds were loaded into each well and left for 2 hr at 4°C until the compounds were diffused. Then the plates were incubated for 24 h at 37 °C. After incubation, the zone of inhibitions was measured and recorded [34, 35].

2.4. Characterizing techniques.

2.4.1. ATR -FTIR measurement.

ATR -FTIR spectral data were collected in the range 4000-400 cm^{-1} using spectrometer VERTEX 80 (Bruker Corporation, Germany) coupled with Platinum Diamond ATR, which consists of a diamond disc as an internal reflection element.

2.4.2. X-ray diffraction measurement.

X-ray diffraction data of the studied samples were measured at ambient temperature using a computer-controlled X-ray diffractometer (PANalytical Empyrean, Netherlands) with Cu kα- radiation (λkα= 1.5406 Å) operated at 30 mA and 45 kV. The powder diffraction patterns were scanned in the 2-theta range of 4°–80°, with scan step 0.026, counting time 40 s/step. A standard quartz sample was used for determining the instrumental profile under the same conditions as the investigated samples for crystallite size and crystallinity index analysis. Data analysis was performed through High Score Plus suit v3 [36] and the WinFit program [377].

2.4.3. Magnetic properties measurement.

Magnetic measurements were conducted by vibrating-sample magnetometer (VSM) model: 7410 series (Lake Shore Cryotronics, USA) at Physics Division, National Research Centre.

3. Results and Discussion

To elucidate their structural properties, a series of chitosan with different weight percentages of magnetite films were analyzed with ATR-FTIR, XRD, and VSM. Then, its antimicrobial activity was assessed against different microorganisms, as in the following.

3.1. ATR- FTIR results.

Figure 1 represents ATR-FTIR spectra of chitosan, Fe_3O_4, and chitosan/ Fe_3O_4 with different weight percentages of Fe_3O_4 (5.0, 10.0, 15.0, and 20.0 wt%). Pure chitosan has an absorption band at 3250 cm^{-1} corresponding to O-H and N-H stretching vibration. Bands at 2924 cm^{-1} and 2875 cm^{-1} are assigned to C-H symmetric and asymmetric stretching vibration, respectively. The stretching vibration of amide I is seen at 1637 cm^{-1}, while the band at 1546 cm^{-1} is related to the amide II band of N-H bending vibration. The bending vibration of the C-H group is seen at 1405 cm^{-1}, 1378 cm^{-1}, and 1321 cm^{-1}. The stretching vibration of the C-O-C group is observed at 1152 cm^{-1}, and bands at 1064 cm^{-1} and 1022 cm^{-1} correspond to skeletal vibration of the stretching vibration of C-O of glucosamine residue. The bending vibration of the O-H group is seen at 648 cm^{-1} and 614 cm^{-1}. The band at 558 cm^{-1} is assigned to the out-of-plane bending of NH and C-O, respectively.

Fe_3O_4 shows bands at 3195 cm^{-1} and 1628 cm^{-1} related to O-H stretching and bending vibration of moisture, respectively [38-42]. Magnetite Fe_3O_4 has two strong infrared absorption bands at 547 cm^{-1} and 435 cm^{-1}, which are assigned to the Fe–O stretching mode of the tetrahedral and octahedral sites (the band at 547 cm^{-1}) and the Fe–O stretching mode of the octahedral sites (the band at 435 cm^{-1}) [43, 44].

For chitosan/ Fe_3O_4 with different weight percentages of Fe_3O_4 (5.0, 10.0, 15.0, and 20.0 wt%), the broadening of the O-H band becomes broader compared to pure chitosan. A new band appeared at 468 cm^{-1} and then shifted toward lower frequency, while its intensity increased with increasing the weight percentage of Fe_3O_4. This confirmed the interaction between chitosan and Fe_3O_4. It is observed that chitosan with a 10.0 weight percentage of Fe_3O_4 has bands of lower intensities compared to another weight percentage of Fe_3O_4. That means this weight percentage of Fe_3O_4 is the most reactive ratio compared to the others.

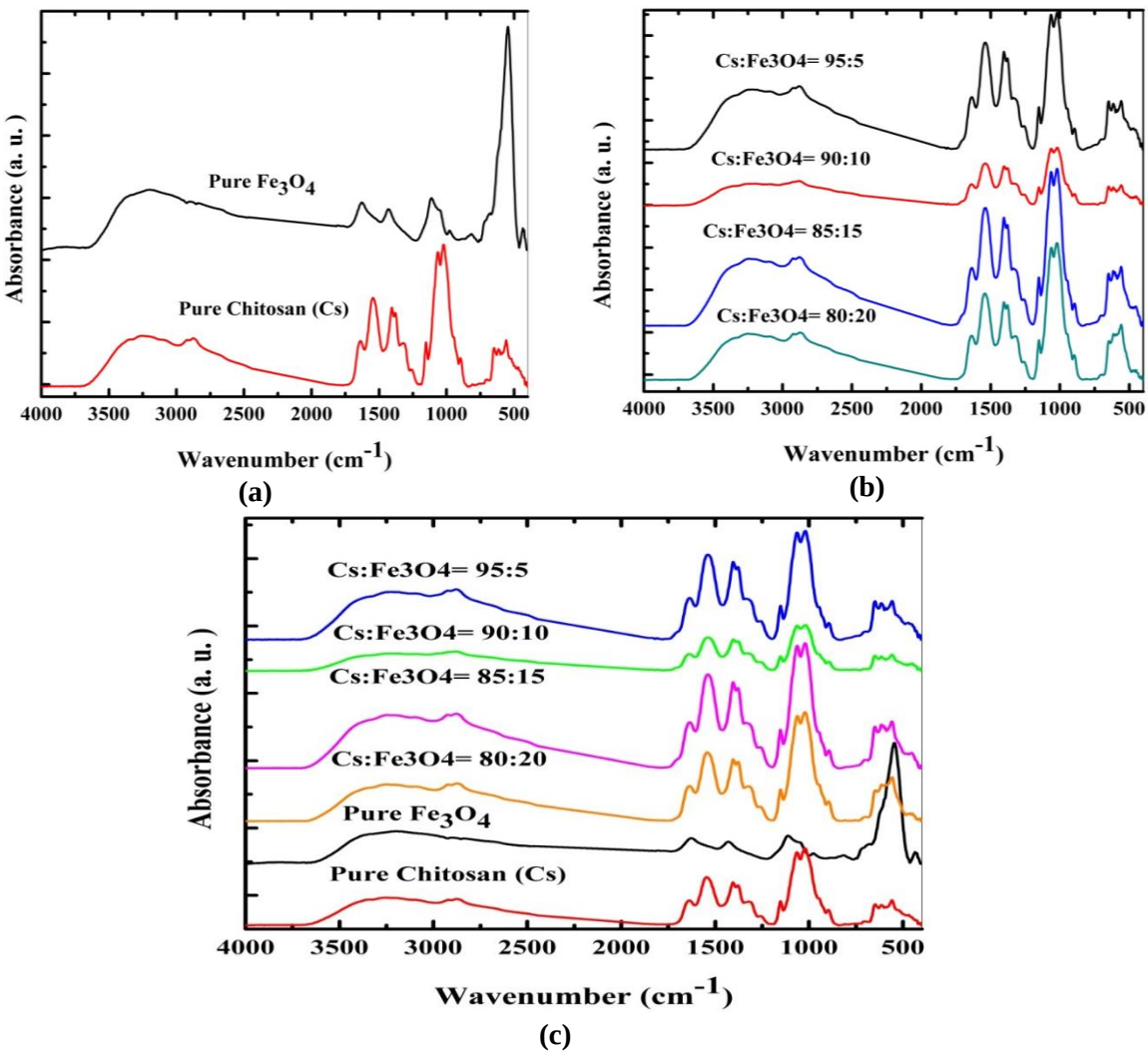

Figure 1. ATR-FTIR absorption spectra of (**a**) Chitosan and Fe_3O_4; (**b**) Chitosan with a different weight percentage of Fe_3O_4 (5.0, 10.0, 15.0 and 20.0 wt%); (c) Chitosan, Fe_3O_4, and chitosan with: 5.0, 10.0, 15.0 and 20.0 wt% of Fe_3O_4.

3.2. X-Ray results

XRD results showed that the chitosan (Fig.2) is well defined according to the chitosan broad peaks around 9°, 11°, and 20°. Also, the magnetite reference card no. 98-015-8742 of the ICDD database (PDF-2, 2010) (Fig.3) matched the most prominent diffraction peak positions of magnetite 35.55°, 43.03°, 57.17°, 62.74° which is consistent with previous literature [45]. The chitosan diffraction peaks became broader compared to pure chitosan and shifted toward higher 2 theta, which can be interpreted by the rearrangement of chitosan chains resulting from the interaction of chitosan with magnetite. These results confirm the interaction, showing that the preparation method gave the chitosan with magnetite as a composition in the same matrix, which is in agreement with previously reported literature [46, 47].

The crystallinity index (CrI) and crystallite size were calculated according to the reported literature using the area under the peaks based on the profile fitting to eliminate the instrumental error [48]. CrI was estimated considering that the peak at 35.55˚ is the most crystalline peak, using the ratio of the area of the crystalline peaks (A cryst) to the total area of the diffraction peaks (Atotal) [%Cr I = 100 × Acryst/ATotal [49]. As indicated in Table 2, the increase in the crystallinity index and crystallite size with increasing the concentration of magnetite indicates that the samples prefer the amorphous form at the low concentrations of

Fe_3O_4, and they rearrange towards the crystalline state due to the presence of magnetite, as the calculations depend on its characteristic crystalline peak. The chitosan has a semi-crystalline nature which is evident in the broadening of the characteristic diffraction peaks. It is noticed that chitosan with a 10.0 weight percentage of magnetite has the broadest peaks of chitosan, which means that this weight percentage is the most reactive ratio compared to the other ratios, which is consistent with FTIR results.

Table 2. Crystallite index and crystallite size in (nm) for chitosan, Fe_3O_4, and chitosan/ Fe_3O_4 with different weight percentages of Fe_3O_4 (5.0, 10.0, 15.0, and 20.0 wt%).

Sample	**Chitosan (Cs) S1**	**Cs: Fe3O4 =95:5 S2**	**Cs: Fe3O4 =90:10 S3**	**Cs: Fe3O4 =85:15 S4**	**Cs: Fe3O4 =80:20 S5**	**Magnetite Fe3O4 S6**
Crystallinity index	0%	0.5 %	1%	5%	9 %	100%
Crystallite size (nm)	1.7	5.2	7.8	8.9	9.5	11.5

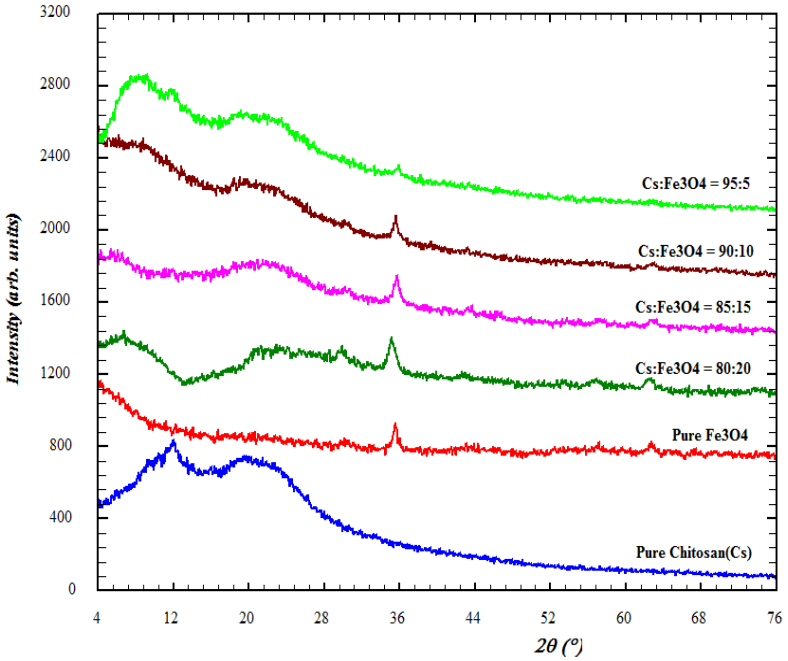

Figure 2. X-ray diffraction patterns of pure chitosan and chitosan with different weight percentages of magnetite.

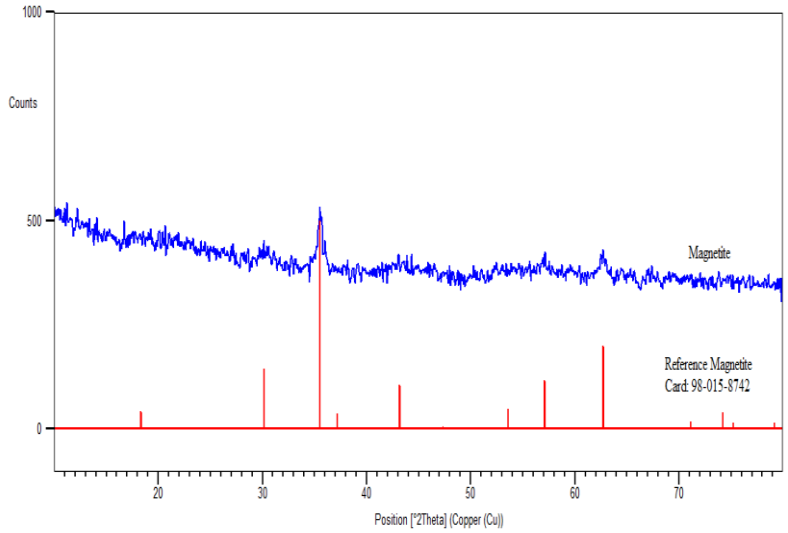

Figure 3. X-ray diffraction patterns of magnetite with reference card no. 98-015-8742.

3.3. Magnetic hysteresis loop results.

Figure 4 presents the changes in the magnetization of chitosan under the influence of a high magnetic field (20 K Oe). This figure shows that pure chitosan has a diamagnetic nature as it has negative susceptibility and that chitosan / Fe_3O_4 nanocomposites are a hard magnetic material and possess unsaturated magnetization even at higher values of the external field. Extrapolating the Moment/Mass-Field curve gives the saturation magnetization for all samples.

Figure 5 shows the magnetization and the higher saturation magnetization value for pure magnetite, which is 66.141 emu/g. The saturation magnetization (M_S), remanent magnetization (M_r), the ratio (SQ = M_r/M_S), and the coercive field (H_C) are listed in Table 3. As listed in the table, the saturation magnetization equals 0.01429 emu/g for pure chitosan and 66.141 emu/g for pure magnetite and increases with increasing magnetite concentration in the samples.

Figure 6 presents the variety of M_S with Fe_3O_4 in chitosan/ Fe_3O_4 nanocomposites; the M_S increased with decreasing the amount of chitosan in the prepared chitosan/ Fe_3O_4 nanocomposites because chitosan is not a magnetic material. This means increasing the amount of Fe_3O_4 to 20 wt.%, causing the M_S to increase. The superparamagnetic behavior of the prepared chitosan/ Fe_3O_4 nanocomposites is displayed by the little values of M_r, M_r/M_S ratio, and H_c. Similarly, the remanent magnetization (M_r) is increased slightly upon adding different amounts of Fe_3O_4 as compared with the undoped sample. The small M_r/M_s values demonstrated a critical part of superparamagnetic particles. On the other hand, H_c of Chitosan decreases with increasing the amount of Fe_3O_4 up to = 10 wt% and then increases slightly at higher Fe_3O_4 concentrations.

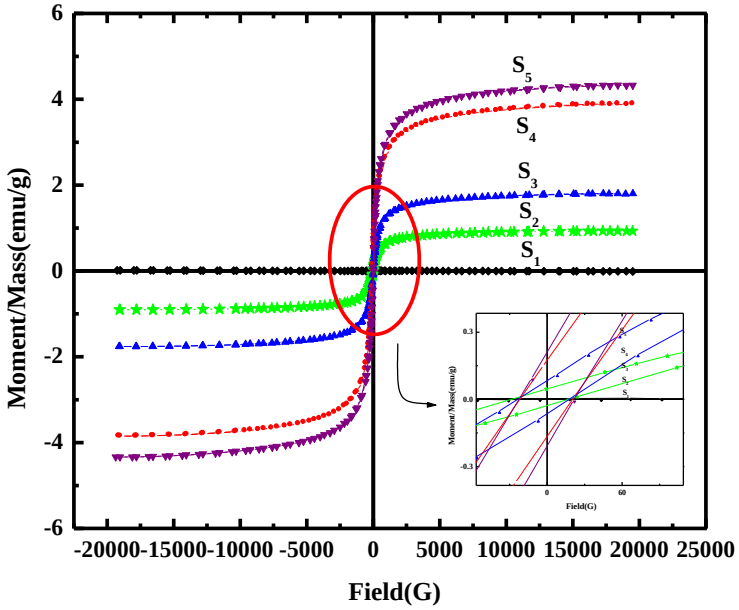

Figure 4. Dependence of magnetization on the applied magnetic field for pure chitosan and chitosan doped with different concentrations of magnetite nanoparticles, focusing on the range of small G to show the existence of different magnetic parameters.

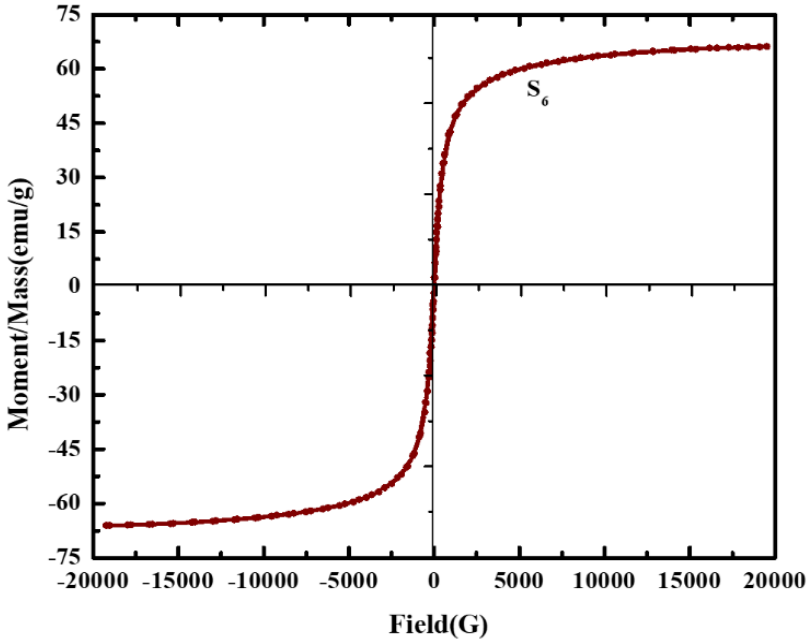

Figure 5. Magmatic moment/mass as a function of applied magnetic field for magnetite.

Table 3. Magnetic parameters for pure chitosan and chitosan with different weight percentages of magnetite at room temperature.

Sample	Ms (emu/g)	Mr(emu/g)	Mr/Ms	Hc (G)
S1	0.01429	0.00148	0.10419	4023.3
S2	0.91896	0.03731	0.04060	22.643
S3	1.7828	0.07397	0.04149	20.629
S4	3.8728	0.17058	0.04404	21.100
S5	4.3316	0.20963	0.04839	22.035
S6	66.141	1.6025	0.02422	17.690

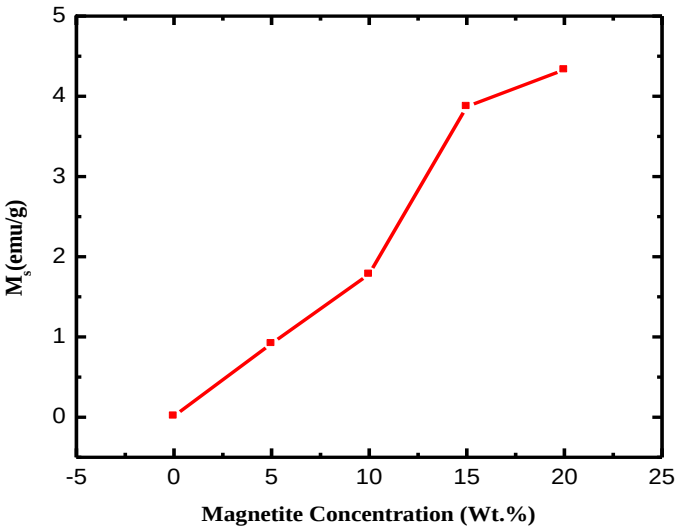

Figure 6. Saturation magnetization as a function of Fe_3O_4 concentration in chitosan/ Fe_3O_4 samples.

The obtained results could dedicate the studied Fe_3O_4/chitosan nanocomposite as an effective tool for magnetic drug targeting. It was stated earlier that such a material could be used for magnetic drug targeting for cancer [50].

3.4. Antimicrobial efficiency (AME) of Fe_3O_4-functionalized nanoparticles.

It is observed that the superoxide and hydroxide in Fe_3O_4 cause the nanoparticles to agglomerate the iron oxide nanoparticles, which often increases the ionic strength, leads to oxidative stress, and damages proteins, membranes, and DNA.

Table 4. Values of zone inhibitions for gram-positive and gram-negative bacteria for Cs/ Fe_3O_4 and Cs/ Fe_3O_4 doped with different weight percentages of Fe_3O_4 NPs.

Sample	Sample Name	Escherichia Coli	Bacillus cereus	Salmonella typhi	Staphylococcus aureus
S1	Cs/Fe3O4 0%	0.18 cm	0.22 cm	0.14 cm	0.20 cm
S2	Cs/Fe3O4 5%	0.20 cm	0.24 cm	0.15 cm	0.23 cm
S3	Cs/Fe3O4 10%	0.24 cm	0.28 cm	0.16 cm	0.28 cm
S4	Cs/Fe3O4 15%	0.25 cm	0.30 cm	0.18 cm	0.29 cm
S5	Cs/Fe3O4 20%	0.27 cm	0.32 cm	0.21 cm	0.31 cm

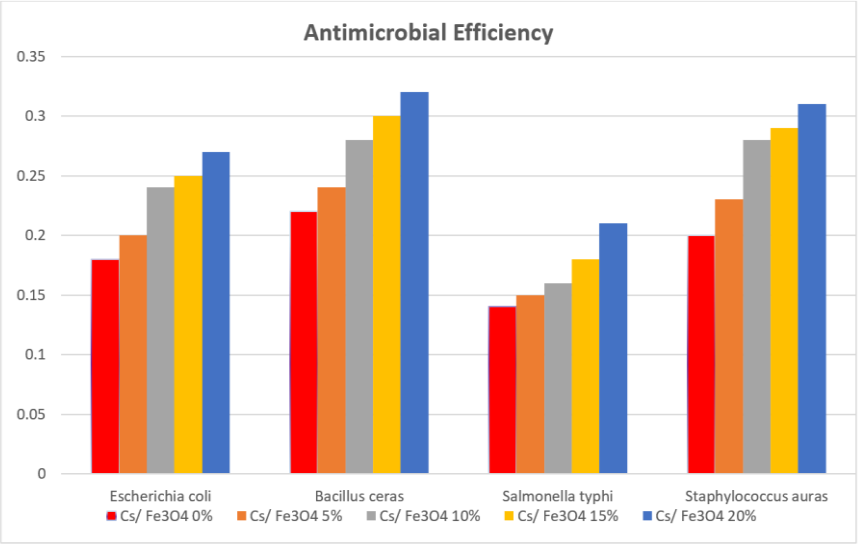

Figure7. Values of zone inhibitions for chitosan and chitosan /Fe_3O_4 with different weight percentages of Fe_3O_4 against different types of bacteria.

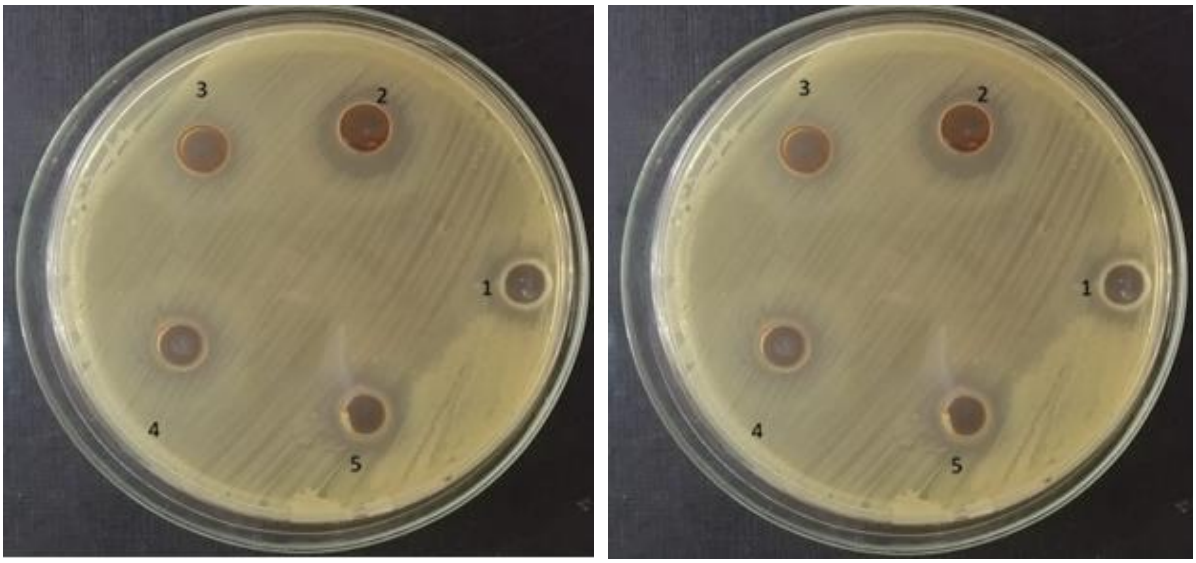

(a) **(b)**

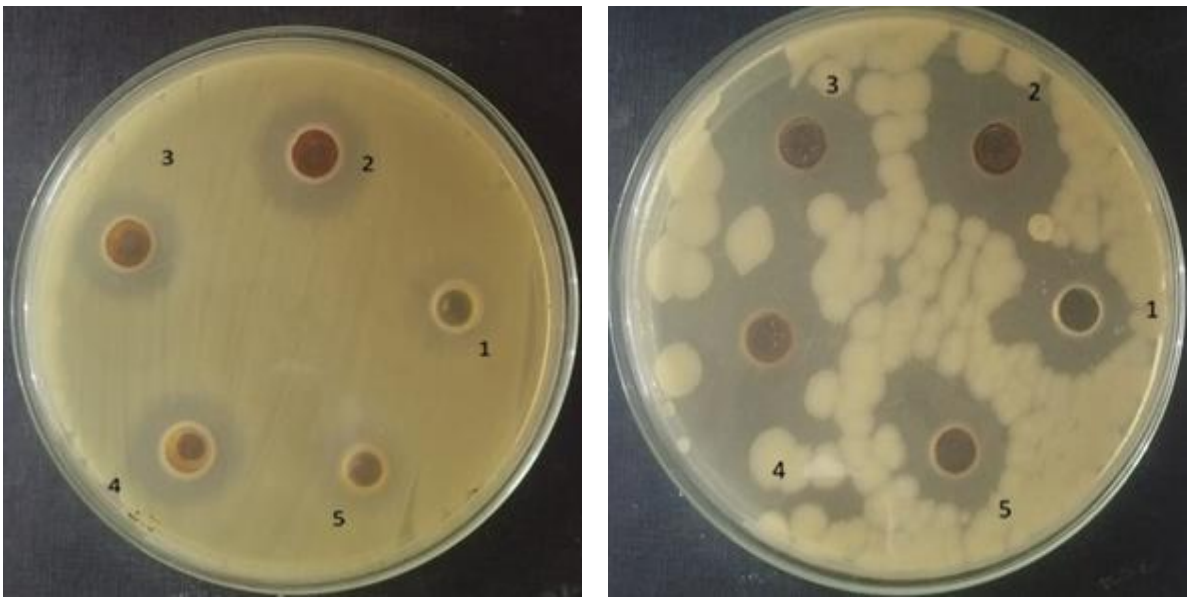

(**c**) (**d**)

Figure 8. Zone of inhibition **(a)** *Staphylococcus aureus*, **(b)** *E. coli*, **(c)** *Salmonella typhi*, and **(d)** *Bacillus cereus*.

In addition, the formation of the bond between the superoxide of the Fe_3O_4 group and the NH_2 group of chitosan increases the activity. It is stated that the antimicrobial effects prevent bacteria growth, which was established previously [51]. The growth kinetic studies of 2 Gram-positive bacteria (*Staphylococcus aureus* 6538 and *Bacillus cereus* ATCC 10987) and 2 Gram-negative bacteria (*Escherichia coli* 8739 and *Salmonella Typhimurium* 14028) in the presence of different concentrations of the negative surface potential of iron oxide nanoparticle (n-IONP) are shown in Table 4. The data indicates a strong antimicrobial propensity of n-IONP against studied bacterial strains. Additionally, the data support the kinetic growth studies observed in Figure 7. Figures 8a and d display the growth zone inhibitions of *B. subtilis* and *S. aureus*, respectively, in the presence of different concentrations of n-IONP. As shown in the figures, there is insignificant growth inhibition compared to *E. coli* (Figure 8b) and *Salmonella Typhi* (Fig. 8c), whereas the inhibition is relatively very dominant. However, measurements indicate the antimicrobial activity of n-IONP *S. aureus*, and *B. cereus* was better than that of *E. coli*, *S. typhi* bacteria shown in Figure 8.

5. Conclusions

Chitosan and chitosan/Fe_3O_4 nanocomposites (IONPs) were synthesized with different concentrations of Fe_3O_4 by the solution casting method. ATR-FTIR of chitosan/ Fe_3O_4 nanocomposites revealed that they undergo a lower frequency shift than pure chitosan, confirming the strong interaction between the matrix and Fe_3O_4.

XRD results revealed that as the concentration of Fe_3O_4 increases in the prepared samples, the crystallinity index (CrI) and crystallite size increase due to the mismatch between the chitosan lattice and that of Fe_3O_4. The saturation magnetization increases as the chitosan amount decreases in the nanocomposites, while the coercivity first decreases and then increases as the amount of Fe_3O_4 increases and as the crystallite size of the nanocomposites increases. Magnetic results confirm the previous findings that dedicate such structure to act as magnetic drug targeting. Finally, the IONPs showed antimicrobial activity against gram-positive bacteria. The bioactivity was noticed strongly in the sample with 10% of F_3O_4 and increased with 15% and 20%.

Funding

We received no funding for this work.

Conflicts of Interest

The authors declare no conflict of interest.

References

1. Rojo, L.; García-Fernández, L.; Aguilar, M. R.; Vázquez-Lasa, B. Antimicrobial polymeric biomaterials based on synthetic, nanotechnology, and biotechnological approaches. *Curr. Opin. Biotechnol***. 2022,** *76*, 102752, https://doi.org/10.1016/j.copbio.2022.102752.
2. Joshi, B.; Khataniar, L.; Bhau, B.S. Chapter 10 - Role of carbon dots in agricultural systems: biotechnology and nanotechnology approach. Editor(s): Khan, R.; Murali, S.; Gogoi, S. *Carbon Dots in Agricultural Systems* **2022**, 225-240, https://doi.org/10.1016/B978-0-323-90260-1.00012-7
3. Li, D.; Liu, Y.; Wu, N. Application progress of nanotechnology in regenerative medicine of diabetes mellitus. *Diabetes Res. Clin. Pract.* **2022**, *190*, 109966, https://doi.org/10.1016/j.diabres.2022.109966
4. Cardoza, C.; Nagtode, V.; Pratap, A.; Mali, S. N. Emerging applications of nanotechnology in cosmeceutical health science: Latest updates. *Health Sciences Review* **2022**, *4*, 100051, https://doi.org/10.1016/j.hsr.2022.100051.
5. Adnane, F.; El-Zayat, E.; Fahmy, H. M. The combinational application of photodynamic therapy and nanotechnology in skin cancer treatment: A review. *Tissue and Cell.* **2022**, *77*, 101856, https://doi.org/10.1016/j.tice.2022.101856.
6. Binandeh M. Performance of unique magnetic nanoparticles in biomedicine. *E. J. ME. CH. Report.* **2022**, *6*, 100072. https://doi.org/10.1016/j.ejmcr.2022.100072.
7. Kolitsi, L.I.; Orova, M.; Yiantsios, S. G. A model of magnetic nanoparticle transport and their effects in tumor areas: Assessment of desirable magnetic properties. *J. Magn. Magn. Mater.* **2022,** *561*, 169732, https://doi.org/10.1016/j.jmmm.2022.169732.
8. Zhang,Z.Q.; Song, S.C. Thermosensitive/superparamagnetic iron oxide nanoparticle-loaded nanocapsule hydrogels for multiple cancer hyperthermia. *Biomaterials* **2016**, *11*, 13–23, https://doi.org/10.1016/j.biomaterials.2016.08.015.
9. Saikia, C.; Das, M.K.; Ramteke, A.; Maji, T.K. Effect of crosslinker on drug delivery properties of curcumin loaded starch coated iron oxide nanoparticles. *Int. J. Biol. Macromol* **2016**, *12*, 1121–1132, https://doi.org/10.1016/j.ijbiomac.2016.09.043.
10. An.Hui, Lu.; Salabas, E.L.; Schüth, F. Magnetic nanoparticles: Synthesis, protection, functionalization, and application. *Angew. Chem. Int. Ed. Engl* **2007**, *46*, 1222–1244, https://doi.org/10.1002/anie.200602866.
11. Rümenapp, C.; Gleich, B.; Haase, A. Magnetic Nanoparticles in Magnetic Resonance Imaging and Diagnostics, *Pharm. Res.* **2012**, *3*, 1165–1179, https://doi.org/10.1007/s11095-012-0711-y.
12. Omar, A.; Badry, R.; Hegazy, M. A.; Yahia, I. S.; Elhaes, H.; Zahran, H.Y.; Ibrahim, M. A.; Refaat, A. Enhancing the Optical Properties of Chitosan, Carboxymethyl Cellulose, Sodium Alginate Modified with Nano Metal Oxide and Graphene Oxide. *Optical and Quantum Electronics* **2022**, *54*, 1-15, https://doi.org/10.21203/rs.3.rs-1079643/v1.
13. Goy, R.C.; Britto, D.d.; Assis, O.B. A review of the antimicrobial activity of chitosan. *Polímeros* **2009**, *3*, 241-247, https://doi.org/10.1590/S0104-14282009000300013.
14. Zeng, H.P.; Yu, Y.P.; Wang, F.S.; Zhang, J.; Li, D. Arsenic(V) removal by granular adsorbents made from water treatment residuals materials and chitosan, *Colloids Surf. A: Physicochem. Eng. Asp., A* **2020**, *1*, 124036, https://doi.org/10.1016/j.colsurfa.2019.124036.
15. Mei, J.F.; Zhang, H.; Mo, S.Q.; Zhang, Y.Z.; Li, Z.Y.; Ou, H.X. Prominent adsorption of Cr(VI) with graphene oxide aerogel twined with creeper-like polymer based on chitosan oligosaccharide, *Carbohydr. Polym.* **2020**, *1*, 116733, https://doi.org/10.1016/j.carbpol.2020.116733.
16. Jianbo, L.; Baixue, L.; Wanlu, L.; Zhang, X.; Zhang, W.; Zhang, P.; Runxi, S.; Dongfang, L. Nano iron oxides impregnated chitosan beads towards aqueous Cr(VI) elimination: Components optimization and performance evaluation, *Colloids and Surfaces A: Physicochemical and Engineering Aspects* **2021**, *11*, 126902, https://doi.org/10.1016/j.colsurfa.2021.126902.

17. Alkahtane, A.A.; Alghamdi, H. A.; Aljasham, A. T.; and Alkahtani, S. A possible theranostic approach of chitosan-coated iron oxide nanoparticles against human colorectal carcinoma (HCT-116) cell line, *Saudi Journal of Biological Sciences* **2022**, *29*, 154-160, https://doi.org/10.1016/j.sjbs.2021.08.078.
18. Arias, L.S.; Pessan, J.P.; deSouzaNeto, F.N.; Lima, B.H.R.; deCamargo, E.R.; Ramage, G.; Delbem, A.C.B.; Monteiro, D.R. Novel nanocarrier of miconazole based on chitosan-coated iron oxide nanoparticles as a nanotherapy to fight Candida biofilms. *Colloids Surf. B* **2020**, *8*, 111080, https://doi.org/10.1016/j.colsurfb.2020.111080.
19. Berry, C.C.; Wells, S.; Charles, S.; Curties, A.S.G. Dextran and albumin derivatised iron oxide nanoparticles: influence on fibroblasts in vitro. *Biomaterials* **2003**, *25*, 4551-4557, https://doi.org/10.1016/S0142-9612(03)00237-0.
20. Park, S.I.; Lim, J.H.; Kim, C.O. Surface-modified magnetic nanoparticles with lecithin for applications in biomedicine. *Curr.Appl.Phys.* **2008**, *6*, 706-709, https://doi.org/10.1016/S0142-9612(03)00237-0.
21. Zhao, G.; Xu, J.J.; Chen, V. Fabrication, characterization of Fe3O4 multilayer film and its application in promoting direct electron transfer of hemoglobin. *Electrochem. Commun*. **2006**, *1*, 148-154, https://doi.org/10.1016/j.elecom.2005.11.001.
22. Tran, N.; Webster, T.j. Magnetic nanoparticles: biomedical applications and challenges. *J. Mater. Chem.* **2010**, *9*, 8760–8767, https://doi.org/10.1039/C0JM00994F.
23. Gupta, AK.; Wells, S., Surface-modified superparamagnetic nanoparticles for drug delivery: preparation, characterization, and cytotoxicity studies. *Nano Bioscience* **2004**, *1*, 66–73, https://ieeexplore.ieee.org/document/1273511.
24. Raafat, D.; Von Bargen, K.; Haas, A.; Sahl, H.G. Insights into the Mode of Action of Chitosan as an Antibacterial Compound. *Appl. Environ. Microbiol*. **2008**, *6*, 3764–3773, https://doi.org/10.1128/AEM.00453-08.
25. Gupta, AK.; Gupta, M., Using hydroxyapatite nanoparticles and decreased crystallinity to promote osteoblast adhesion similar to functionalizing with RGD. *Biomaterials* **2005**, *14*, 3995–4021, https://doi.org/10.1016/j.biomaterials.2005.12.008.
26. Niemirowicz, K.; Markiewicz, K.H.; Wilczewska, A.Z.; Car,H. Magnetic nanoparticles as new diagnostic tools in medicine. *Advances in Medical Sciences* **2012**, *57*, 196-207, https://doi.org/10.2478/v10039-012-0031-9.
27. Braim, F. S.; Ashikin Nik Ab Razak, N. N.; Abdul Aziz, A.; Ismael, L. Q.; Sodipo, B. K. "Ultrasound assisted chitosan coated iron oxide nanoparticles: Influence of ultrasonic irradiation on the crystallinity, stability, toxicity and magnetization of the functionalized nanoparticles. *Ultrasonics Sonochemistry* **2022**, *8*, 106072, https://doi.org/10.1016/j.ultsonch.2022.106072.
28. Hassani, S.; Gharehaghaji, N.; Divband, B. Chitosan-coated iron oxide/graphene quantum dots as a potential multifunctional nanohybrid for bimodal magnetic resonance/fluorescence imaging and 5-fluorouracil delivery. *Materials today communications* **2022**, *7*, 103589, https://doi.org/10.1016/j.mtcomm.2022.103589.
29. Giglou, M. T.; Giglou, R. H.; Esmaeilpour, B.; Azarmi, R.; Padash, A.; Falakian, M.; Śliwka, J.; Gohari G.; Lajayer, H. M. A new method in mitigation of drought stress by chitosan-coated iron oxide nanoparticles and growth stimulant in peppermint. *Ind Crops Prod*. **2022**, *11*, 115286, https://doi.org/10.1016/j.indcrop.2022.115286.
30. Cai, Y.; Karmakar, B.; Salem, M. A.; Alzahrani, A. Y.; Bani-Fwaz, M. Z.; Oyouni, A. A. A.; Al-Amer, O.; Batiha, G. E. Ag NPs supported chitosan-agarose modified Fe_3O_4 nanocomposite catalyzed synthesis of indazolo[2,1-b]phthalazines and anticancer studies against liver and lung cancer cells. *Int. J. Biol. Macromol.* **2022,** *208*, 20-28, https://doi.org/10.1016/j.ijbiomac.2022.02.172.
31. Liandi, A. R.; Cahyana, A. H.; Yunarti, R. T.; Wendari, T. P. Facile synthesis of magnetic Fe_3O_4@Chitosan nanocomposite as environmentally green catalyst in multicomponent Knoevenagel-Michael domino reaction. *Ceram. Int.* **2022**, *48*, 20266-20274, https://doi.org/10.1016/j.ceramint.2022.03.307.
32. Roy, N.; Kannabiran, K.; Mukherjee, A. Studies on photocatalytic removal of antibiotics, ciprofloxacin and sulfamethoxazole, by Fe_3O_4-ZnO-Chitosan/Alginate nanocomposite in aqueous systems. *Adv. Powder Technol.* **2022,** *33*, 103691, https://doi.org/10.1016/j.apt.2022.103691.
33. Kaveh, R.; Bagherzadeh, M. Simultaneous removal of mercury ions and cationic and anionic dyes from aqueous solution using epichlorohydrin cross-linked chitosan @ magnetic Fe_3O_4/activated carbon nanocomposite as an adsorbent. *Diam. Relat. Mater.* **2022,** *124*, 108923, https://doi.org/10.1016/j.diamond.2022.108923.

34. Gamal, M.El.; Saad, A.M. Sh.; Mohammed, H. Antimicrobial activities and cytotoxicity of Sisymbriumirio L extract against Multi-Drug Resistant Bacteria (MDRB) and Candida albicans. *Int. J. Curr. Microbiol. Appl. Sci*. **2017**, *6*, 1-13, https://doi.org/10.20546/ijcmas.2017.604.001.
35. Clinical Laboratory Standards Institute (CLSI). Performance Standards for Antimicrobial Susceptibility Testing, **2017**, *27*, Replaces M100-S26, https://clsi.org/media/1469/m100s27_sample.pdf.
36. Degen, T.; Sadki, M.; Bron, E.; König, U.; Nénert, G. The High Score suite, Powder Diffraction, *Technical Artic ale* **2014**, *29*, S13-S18, https://www.malvernpanalytical.com/powder/diffractometer.
37. Krumm, S., An Interactive Windows Program for Profile Fitting and Size/Strain Analysis. *Materials Science Forum* **1996**, 228-231, https://doi.org/10.4028/www.scientific.net/MSF.228-231.183.
38. Romainor, A.N.B.; Chin, S. F. S.; Pang, C. L.; Bilung,M. Preparation and characterization of chitosan nanoparticles-doped cellulose films with antimicrobial property. *J. Nanomater*. **2014**, *1*, 130, https://doi.org/10.1155/2014/710459.
39. Varma, R.; Vasudevan, S. Extraction, Characterization, and Antimicrobial Activity of Chitosan from Horse Mussel Modiolus modiolus. *ACS Omega* **2020**, *5*, 20224-20230, https://pubs.acs.org/doi/full/10.1021/acsomega.0c01903.
40. Kumar, S.; Koh, J.; Kim, H.; Gupta, M.K.; Dutta, P.K. A new chitosan–thymine conjugate: Synthesis, characterization and biological activity. *Int. J. Biol. Macromol*. **2012**, *50*, 493-502, https://doi.org/10.1016/j.ijbiomac.2012.01.015.
41. El-Hefian, E. A.; Nasef, M.M.; Yahaya, A.H. The preparation and characterization of chitosan/poly (vinyl alcohol) blended films. *E-J Chem.* **2010**, *7*, 1212-1219, https://doi.org/10.1155/2010/626235.
42. El-Sayed, S. T.; Ali, A.M.; El-Sayed, E.M.; Shousha, W.G.; Omar, N.I. Characterization and potential antimicrobial effect of novel chitooligosaccharides against pathogenic microorganisms. *J. Appl. Pharm. Sci.* **2017**, *2*, 6-12, https://japsonline.com/abstract.php?article_id=2287.
43. Stoia, M.; Istratie, R.; Păcurariu, C. Investigation of magnetite nanoparticles stability in air by thermal analysis and FTIR spectroscopy. *J Therm Anal Calorim.* **2016**, *125*, 1185-1198, https://link.springer.com/article/10.1007/s10973-016-5393.
44. Bordbar, A. K.; Rastegari, A.A.; Amiri, R.; Ranjbakhsh, E.; Abbasi, M.; Khosropour, A.R. Characterization of modified magnetite nanoparticles for albumin immobilization. *Biotechnol Res Int.* **2014**, *5*, 6, http://dx.doi.org/10.1155/2014/705068.
45. Jamshidiyan, M.; Shirani, A.S.; Alahyarizadeh, G. Solvothermal synthesis and characterization of magnetic Fe3O4 nanoparticle by different sodium salt sources. *Mater. Sci-Poland* **2017**, *35*, 50-57, https://doi.org/10.1515/msp-2017-0004.
46. Ma,B.; Hou, X.; He, C. Preparation of Chitosan Fibers Using Aqueous Ionic Liquid as the Solvent. *Fiber Polym.* **2015**, *16*, 2704-2708, https://link.springer.com/article/10.1007/s12221-015-5638-6.
47. Kefeni, K. K.; Msagati, T. A. M.; Mamba, B.B. Ferrite nanoparticles: synthesis, characterization and applications in electronic device, *Materials Science and Engineering: B* **2017**, *6*, 37–55, https://doi.org/10.1016/j.mseb.2016.11.002.
48. Osorio, M. A.; David, L.; Trombotto, S.; Lucas, L.M.; Peniche, C.C.; Domard, A. Kinetics study of the solid-state acid hydrolysis of chitosan: Evolution of the crystallinity and macromolecular structure. *Biomacromolecules* **2010**, *11*, 1376–1386, https://doi.org/10.1021/bm1001685.
49. Arias, J.L.; Reddy, L. H.; Couvreur,P. Fe_3O_4/chitosan nanocomposite for magnetic drug targeting to cancer. *J. Mater. Chem*. **2012**, *22*, 7622-7632, https://pubs.rsc.org/en/content/articlehtml/2012/jm/c2jm15339.
50. Mukherje, M. In vitro antimicrobial activity of polyacrylamide doped magnetic iron oxide nanoparticles. *Int. J. Mater. Mech. Manuf.* ***2014***, *2*, 64 –66, https://doi.org/10.7763/IJMMM.2014.V2.101.
51. Ramteke, C.; Sarangi, B.K.; Chakrabarti, T.; Mudliar, S.; Satpute, D.; Pandey, R.A. Synthesis and broad spectrum antibacterial activity of magnetite ferrofluid. *Curr. Nanosci.* **2010**, *6*, 587–591, https://doi.org/10.2174/157341310793348605.